Journal of Solid State Chemistry 183 (2010) 532–541

Contents lists available at ScienceDirect

Journal of Solid State Chemistry

journal homepage: www.elsevier.com/locate/jssc

On the ammonolysis of Ga_2O_3: An XRD, neutron diffraction and XAS investigation of the oxygen-rich part of the system Ga_2O_3–GaN

D. Roehrens, J. Brendt, D. Samuelis [1], M. Martin *

Institute of Physical Chemistry, RWTH Aachen University, Landoltweg 2, 52056 Aachen, Germany

ARTICLE INFO

Article history:
Received 18 August 2009
Received in revised form
19 December 2009
Accepted 26 December 2009

Dedicated to Prof. Dr. Rüdiger Kniep on the occasion of his 65th birthday
Available online 4 January 2010

Keywords:
β-Ga_2O_3
GaN
Ammonolysis
Oxynitrides
Nitrogen solubility

ABSTRACT

We investigated the ammonolysis of β-Ga_2O_3 at elevated temperatures by means of *ex situ* X-ray diffraction, *ex situ* neutron diffraction and *in situ* X-ray absorption spectroscopy. Within the detection limits of these methods, we can rule out the existence of a crystalline or amorphous oxynitride phase that is not derived from wurtzite-type GaN. No evidence for a β-Ga_2O_3 related oxynitride phase was found, and the nitrogen solubility in β-Ga_2O_3 was found to be below the detection limit of about 2–3 at% in the anionic sublattice. These findings were obtained by monitoring the anionic occupancy factors and the lattice parameters of the β-Ga_2O_3 phase obtained from total diffraction pattern refinement with the Rietveld method and by linear combination fitting of the X-ray absorption spectra that were recorded during the ammonolysis.

1. Introduction

1.1. Background

Recent developments have shown increased interest in gallium oxide and gallium nitride compounds as base materials for (opto-) electronic components such as light emitting diodes or sensors [1–5]. While there have been extensive efforts in researching the binary compounds β-Ga_2O_3 and GaN, there is only a smaller number of reports on gallium oxynitrides, that are intermediate compounds in the pseudo-binary system GaN–Ga_2O_3. Most of these studies focus on compounds located at the nitrogen-rich side of this system. These oxynitrides are characterized as being derived from wurtzite-type GaN, with dissolved oxygen in the anionic sublattice. It is known, that the anion sublattice of GaN can accommodate up to 30 at% of oxygen, which is—according to the literature—compensated by electrons [6–13] and/or gallium vacancies [14].

Only a few reports exist on oxynitrides that are not derived from GaN. Among them are theoretical studies and high-pressure syntheses of a spinel-type compound, Ga_3O_3N, with a mixed anionic sublattice, which is thermodynamically stable only at high pressure [15–19]. Further reports postulate the existence of gallium oxynitrides as reaction intermediates during the ammonolysis of various gallium oxide modifications [20,21]. Recently, we could show that during the growth of amorphous, gallium oxide by means of pulsed laser deposition (PLD) in a nitrogen-rich atmosphere the quasi-binary system GaN–Ga_2O_3 is left. The resulting gallium oxynitride is anion deficient and contains several percent of nitrogen. In these new materials an insulator–metal transition can be observed during crystallization of stoichiometric β-Ga_2O_3 [22].

Lately, we investigated the *kinetics* of the ammonolysis of Ga_2O_3 and the oxidation of GaN by means of *in situ* X-ray absorption spectroscopy (XAS) [23]. The kinetics of the ammonolysis of Ga_2O_3 can be described very well by a Johnson–Mehl–Avrami–Kolmogorow model with an Avrami-exponent of $\sim$3 indicating a reaction mechanism with closed nucleation of GaN and 3-dimensional nucleus growth. The rate determining step of the reaction is the formation of the newly formed GaN phase at the interface between the GaN nuclei and the Ga_2O_3 matrix. These kinetic results were supported by SEM micrographs which show a severe change of the morphology of the reactants and by TEM micrographs which directly image isolated GaN nuclei that grew during the ammonolysis. The oxidation kinetics of GaN could be modeled by a shrinking core model with cylindrical powder particles whose morphology does not change during the reaction. Again the rate determining step is the interfacial formation of the newly formed gallium oxide product phase.

* Corresponding author. Fax: +49 241 80 92128.
E-mail address: martin@rwth-aachen.de (M. Martin).
[1] Present address: Max Planck Institute for Solid State Research, Heisenbergstr. 1, 70569 Stuttgart, Germany.

0022-4596/$ - see front matter © 2010 Elsevier Inc. All rights reserved.
doi:10.1016/j.jssc.2009.12.024

In continuation of the above, kinetic study, this investigation aims at the detailed characterization of the reactants during the ammonolysis of stoichiometric β-Ga_2O_3 powder samples, focusing on the oxygen-rich side of the system Ga_2O_3–GaN. We used *ex situ* X-ray and neutron diffraction methods and *in situ* X-ray absorption (XAS) experiments in order to detect crystalline or amorphous oxynitride intermediates that may be formed during the reaction. Special emphasis was placed upon the determination of the solubility of nitrogen in the monoclinic β-Ga_2O_3 lattice. Incorporation of nitrogen into the oxide is expected to significantly alter the physico–chemical properties of the material. β-Ga_2O_3 is known to be a wide band gap, n-type semiconductor with a band gap of 4.9 eV [24]. If we assume that dissolved nitrogen exists within Ga_2O_3 as N^{3-} ion, charge compensation of N'_O (Kröger–Vink notation) could be achieved by either oxygen vacancies $V_O^{\bullet\bullet}$, electron holes $h^{\bullet}$, or gallium interstitials $Ga_i^{n\bullet}$ (n=1,2,3), as can be seen from the charge neutrality in Eq. (1).

$$[N'_O]+[e']=2[V_O^{\bullet\bullet}]+[h^{\bullet}]+n[Ga_i^{n\bullet}] \quad (1)$$

Eq. (1) shows that dissolved nitrogen would act as an acceptor. Thus a significant dopant fraction N'_O exceeding the fraction of electrons e' would change the defect structure of Ga_2O_3 and could possibly lead to p-type behavior.

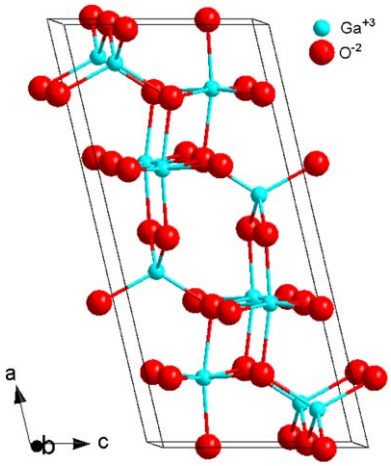

Fig. 1. Crystal structure of β-Ga_2O_3 from crystallographic data determined by Åhman et al. [27].

1.2. Structural information

1.2.1. β-Ga_2O_3

Under standard conditions β-Ga_2O_3 is the thermodynamically stable phase in the Ga–O system [25,26]. It crystallizes in the monoclinic crystal system ($C2/m$). There are two cation positions, one octahedrally and the other tetrahedrally coordinated. For the anion sites there are three crystallographically different positions, with two oxygen ions coordinated trigonally and one tetrahedrally. The structure is shown in Fig. 1 and crystallographic data are summarized in Table 1.

1.2.2. GaN

Under standard conditions α-GaN is the thermodynamically stable phase in the Ga–N system [28]. It crystallizes in the hexagonal wurtzite structure in which both Ga and N atoms are coordinated tetrahedrally. The structure is shown in Fig. 2 and crystallographic data are summarized in Table 2.

2. Experimental

In order to examine for the potential existence of gallium oxynitrides and the solubility of nitrogen in β-Ga_2O_3 we have chosen the ammonolysis of β-Ga_2O_3, which is an established

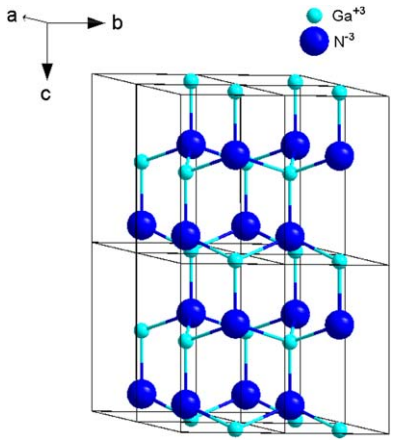

Fig. 2. Crystal structure of GaN from crystallographic data determined by Juza and Hahn [29].

Table 1
Crystallographic data for β-Ga_2O_3 according to Åhman et al. [27]

Phase			β-Ga_2O_3		
Crystal system			Monoclinic		
Space group			$C2/m$		
a [Å]			12.214 (3)		
b [Å]			3.0371 (9)		
c [Å]			5.7981 (9)		
Beta			103.83 (2)		
Cell volume [Å^3]			208.8		
Formula units			4		
General multiplicity			8		
Atom	Wyckoff position	x	y	z	Site occupancy factor
Ga1	4i	0.09050 (2)	0.0	0.79460 (5)	1
Ga2	4i	0.15866 (2)	0.5	0.31402 (5)	1
O1	4i	0.1645 (2)	0.0	0.1098 (3)	1
O2	4i	0.1733 (2)	0.0	0.5632 (4)	1
O3	4i	−0.0041 (2)	0.5	0.2566 (3)	1

Table 2
Crystallographic data for α-GaN according to Juza and Hahn [29]

Phase			GaN		
Crystal system			Hexagonal		
Space group			$P6_3mc$		
a [Å]			3.180 (4)		
b [Å]			3.180 (4)		
c [Å]			5.166 (5)		
Cell Volume [Å^3]			45.2		
Formula units			2		
General multiplicity			12		
Atom	Wyckoff position	x	y	z	Site occupancy factor
Ga	2b	1/3	2/3	0	1
N	2b	1/3	2/3	3/8	1

route of converting gallium oxide into gallium nitride (see [30] as an example). For the qualitative phase analysis and the monitoring of the lattice parameters during ammonolysis we conducted *ex situ* XRD experiments on quenched powder samples. To detect any nitrogen within the ammonolyzed β-Ga_2O_3-phase, *ex situ* neutron diffraction experiments on quenched powder samples were carried out. To take into account the possibility of non-crystalline intermediates during the reaction we monitored the ammonolysis by means of *in situ* X-ray absorption spectroscopy.

2.1. Synthesis

A stoichiometric formulation of the ammonolysis reaction is given in Eq. (2).

$$Ga_2O_3(s)+2NH_3(g)\rightarrow 2GaN(s)+3H_2O(g) \quad (2)$$

Commercially available Ga_2O_3 often consists of a mixture of the α- and β-phases. The β-phase is the thermodynamically stable modification, with a formation Gibbs energy that surpasses that of corundum. Additionally the γ-, δ-, and ε-Ga_2O_3 phases are known. However, for temperatures above 870 °C all these modifications transform to the stable β-phase [25,26]. In our experiments, all powder samples were prepared from commercially available Ga_2O_3 powder (Alfa Aesar, Puratronic) by pre-sintering for 48 h at 1325 °C in air to ensure phase purity of the β-phase and to increase the crystallite size to a level where diffraction line broadening is negligible.

Ammonolysis of the samples used for XRD analysis was carried out in a tubular reactor made up of quartz, and the powder sample was placed in an alumina boat. The temperature at the sample was measured with a conventional type-S thermocouple, sealed in quartz. The sample was heated up to 600 °C under a flow of nitrogen (20 sccm/min). After thermal equilibrium was reached the gas flow was switched to pure ammonia (25 sccm/min). At the end of the reaction time, the gas flow was switched back to nitrogen (20 sccm/min), and the sample was allowed to cool to room temperature (typically a temperature of 100 °C was reached after 2 h).

The samples used for neutron diffraction were prepared in a different reactor which is optimized for larger sample volumes and homogeneity of temperature in a given volume increment. This reactor consists also of a quartz tube that is arranged in a vertical position, but there is an additional heating wire, and there are two chambers that are separated by permeable glass frits. The first chamber was filled with quartz balls of 2 mm radius to ensure an optimal heat transfer onto the gas stream. The samples of about 10 g each were placed onto the second glass frit. The gas mixture passed through the frits and the powder sample with flow rates of 100 sccm/min NH_3 during reaction and 20 sccm/min N_2 during heating/cooling. At the end of the reaction time the sample was allowed to cool down to room temperature (a temperature of 100 °C was reached after about 2.5 h). In order to decrease the reaction time and allow for an easier comparison with the *in situ* XAS data, a higher reaction temperature of 780 °C (compared to the XRD experiments) was chosen for this set of samples.

2.2. X-ray and neutron diffraction

Conventional X-ray diffraction techniques were used to characterize the crystalline samples. Diffraction patterns were recorded on a transmission diffractometer (Stadi-P, STOE Darmstadt, Germany) that is equipped with a primary Ge (111) monochromator and a scintillation counter with graphite secondary monochromator. All measurements were performed with Cu $K\alpha_1$ radiation (λ=1.540598 Å). The XRD patterns were collected in a 2θ-range from 10–120° in steps of 0.05° in order to ensure a sufficient quality of the refinement.

Constant wavelength neutron diffraction was carried out at the SPODI neutron powder diffractometer at the FRMII reactor in Garching, Germany. It is equipped with a vertically focusing monochromator that consists of 17 Ge (551) crystals and 80 ^{3}He detectors. A 2θ-range of 160° is covered, and the diffraction data were afterwards corrected for beam divergence.

Rietveld refinement of XRD and neutron data was carried out with the Fullprof software package using the Thompson–Cox–Hastings Pseudo-Voigt profile function [31]. For each experimental setup, a preceding profile matching routine was applied. The profile parameters thus acquired were used as starting values for each structural refinement. From the pattern matching calculations we extracted the refined lattice parameters, while the quantitative phase composition and atomic parameters where obtained from the structural refinements. The background was fitted as linear interpolation between a set of chosen background points with refineable heights. The neutron wavelength was refined with a standard sample to λ=1.547466(9) Å.

2.3. X-ray absorption spectroscopy

The *in situ* XAS measurements were conducted at the synchrotron DORIS at HASYLAB (Hamburger Synchrotron-Strahlungslabor) at beamlines E4 and C. Measurements were done on the Ga *K*-edge (E_0=10 367 eV) in transmission XAS-geometry, using ionization chambers as detectors and Si-(111)-double crystal monochromators. For filtering higher harmonics, the monochromator was detuned to 60% of the maximum intensity. Additional elements of the monochromators are angle encoder systems for getting an independent energy scale. The ionization

chambers are filled with 10% Ar/N_2 and pure Ar. As energy reference a pellet of the intermetallic compound CoGa [32], diluted with BN, was used.

The XAS measurements were carried out under *in situ* conditions in a furnace specially developed for *in situ* transmission XAS measurements. The furnace consists of a corundum tube (diameter=14 mm, length=250 mm) with surrounding platinum heating wire, which allows to operate the furnace up to temperatures of 1200 °C [33]. Water cooled flanges with Kapton windows allow the X-rays to pass the furnace. Flow rates of He and NH_3 were controlled by two 100 ml min^{-1} mass flow controllers. For more details about the experimental setup see reference [23].

About 5 mg gallium oxide powder was mixed with 40 mg boron nitride powder to obtain the optimal sample amount for our setup. BN windows were used to hold the powder in place. Transport of the gases to the powder particles was ensured by holes in the sample holder, consisting of MACOR-ceramics, while the gas-flow rate was kept constant at 30 sccm/min in each experiment.

The *in situ* spectra were recorded on the gallium *K*-edge in an energy range from 10167-11267 eV. Two different measurement modes were used. QEXAFS [34] was used to analyze the reaction kinetics *in situ* and continuously [23]. However, to record structural changes, longer data acquisition times were necessary. Thus the reaction was quenched after 5 min by changing the gas atmosphere to helium, and then conventional step-scanning XAS was used. After recording the spectrum, another 5 min reaction/XAS acquisition cycle was carried out, until at least 5 consecutive spectra showed no further changes.

XAS raw data analysis was done with the program Athena [35], according to the standard procedures [36]. Smoothing was performed with a 3-point adjacent averaging cycle with three iterations. The energy scale was aligned to the inflection point of a CoGa spectrum with $E_0(CoGa)=E_0(Ga)=10367$ eV. EXAFS background removal was done with the AutoBK algorithm and Rbkg=1.0 Å [37]. Fourier transformation of the k^3-weighted $\chi(k)$ was done with a Kaiser–Bessel window function and a *k*-range from 2.6 to 12.5 $Å^{-1}$.

3. Results and discussion

Ammonolysis reactions of β-Ga_2O_3 were performed at T=600 °C for durations between 1 and 48 h, and the products have been analyzed with XRD. A second set of samples was ammonolyzed at 780 °C for durations between 0 and 2 h and analyzed by *ex situ* neutron diffraction. The *in situ* XAS experiments were conducted at temperatures of 660, 780 and 840 °C.

All powders appear to be of homogenous crystallinity and color before and after the ammonolysis, but the color changes from white to yellow with increasing reaction time. Since GaN is a dark yellow powder, this color change can probably be attributed to the formation of the nitride phase. It has to be noted, however, that all of the ammonolyzed samples are of yellow color and that the intensity of the color seems to correlate with the reaction time, even in cases where only β-Ga_2O_3 can be observed by diffraction means.

3.1. X-ray diffraction data and refinement

The X-ray diffraction patterns of ammonolyzed and subsequently quenched samples are depicted in Fig. 3. They show the evolution of the wurtzite-type nitride phase GaN (space group: $P6_3mc$) with time. Besides the monoclinic β-Ga_2O_3 (space group $C2/m$) and hexagonal GaN no other phases can be detected in the diffraction patterns. This indicates that the transition from β-Ga_2O_3 to GaN does not proceed via (meta-)stable *crystalline* intermediates as had been suggested earlier [20,21].

In order to acquire indirect information about a possible solubility of nitrogen in the monoclinic β-Ga_2O_3 cell we refined each diffraction pattern and focused on the lattice parameters of

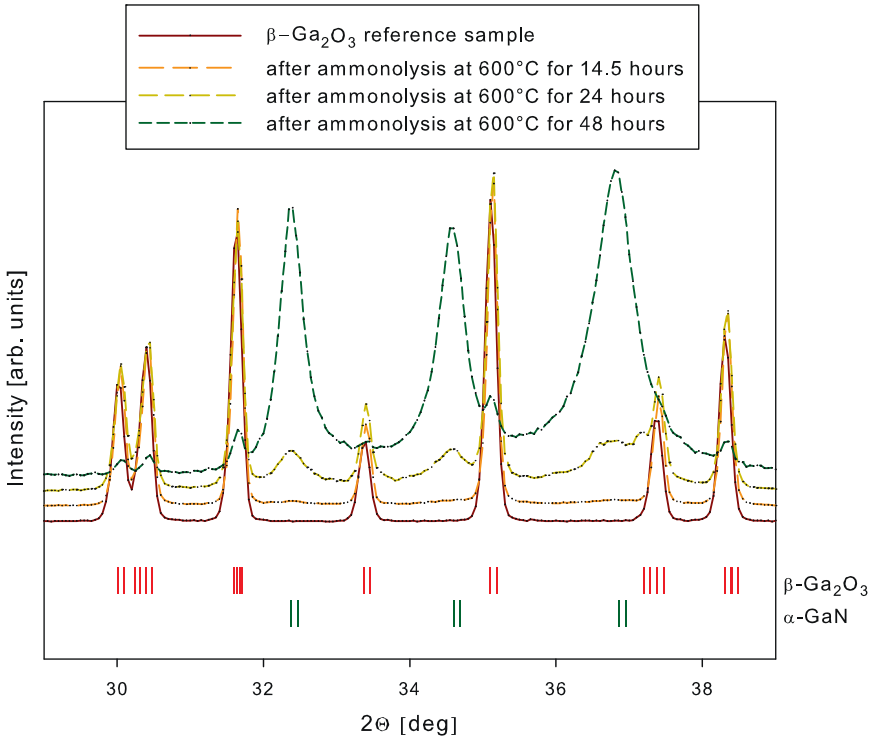

Fig. 3. XRD patterns of β-Ga_2O_3 powder samples ammonolyzed for increasing duration at 600 °C. GaN is first observed after 14.5 h. Patterns taken between 1 and 14.5 h reaction time show exclusively β-Ga_2O_3 reflections and are not shown in this figure.

the oxide phase as an indicator of a possible doping effect. Before we discuss the results, we note that the profile of the evolving nitride phase shows significant particle size related peak broadening effects and the obtained intensity ratios deviate significantly from the theoretical values, which could be indicative of texture effects. This results in an overall decrease of the scattering properties of the powder samples and a significant negative impact on the quality of the refinement. From the Y profile parameter it is possible to extract the volume weighted average particle size, which shows the nitride phase to be nanocrystalline, e.g. with $\langle D \rangle_V = (20 \pm 5)$ nm in sample 5, assuming spherical particles. This is confirmed by the application of the same method

Table 3
Refined cell parameters of the monoclinic β-Ga_2O_3 phase and amount of GaN in samples that were ammonolyzed at 600 °C for different durations, as obtained by XRD (n.d.: not detectable)

Sample	Ammonolysis duration at 600 °C [h]	Rwp	χ^2	Mol% GaN	Cell Volume [Å^3]	a [Å]	b [Å]	c [Å]
1	0	7.27	3.08	n.d.	215.23471 (31)	12.21644 (18)	3.0365 (5)	5.80222 (9)
2	3	6.55	1.52	n.d.	215.45453 (24)	12.21740 (14)	3.03820 (3)	5.80446 (7)
3	6	6.85	2.24	n.d.	215.46331 (22)	12.21797 (13)	3.03827 (3)	5.80427 (6)
4	14.5	6.22	2.12	10.03 (0.27)	215.31308 (20)	12.21427 (11)	3.03778 (3)	5.80291 (5)
5	24	9.50	3.54	59.54 (0.84)	215.45645 (44)	12.21613 (27)	3.03869 (6)	5.80417 (11)
6	48	14.8	8.37	96.12 (1.44)	215.64534 (54)	12.2153 (28)	3.03840 (10)	5.8101 (15)

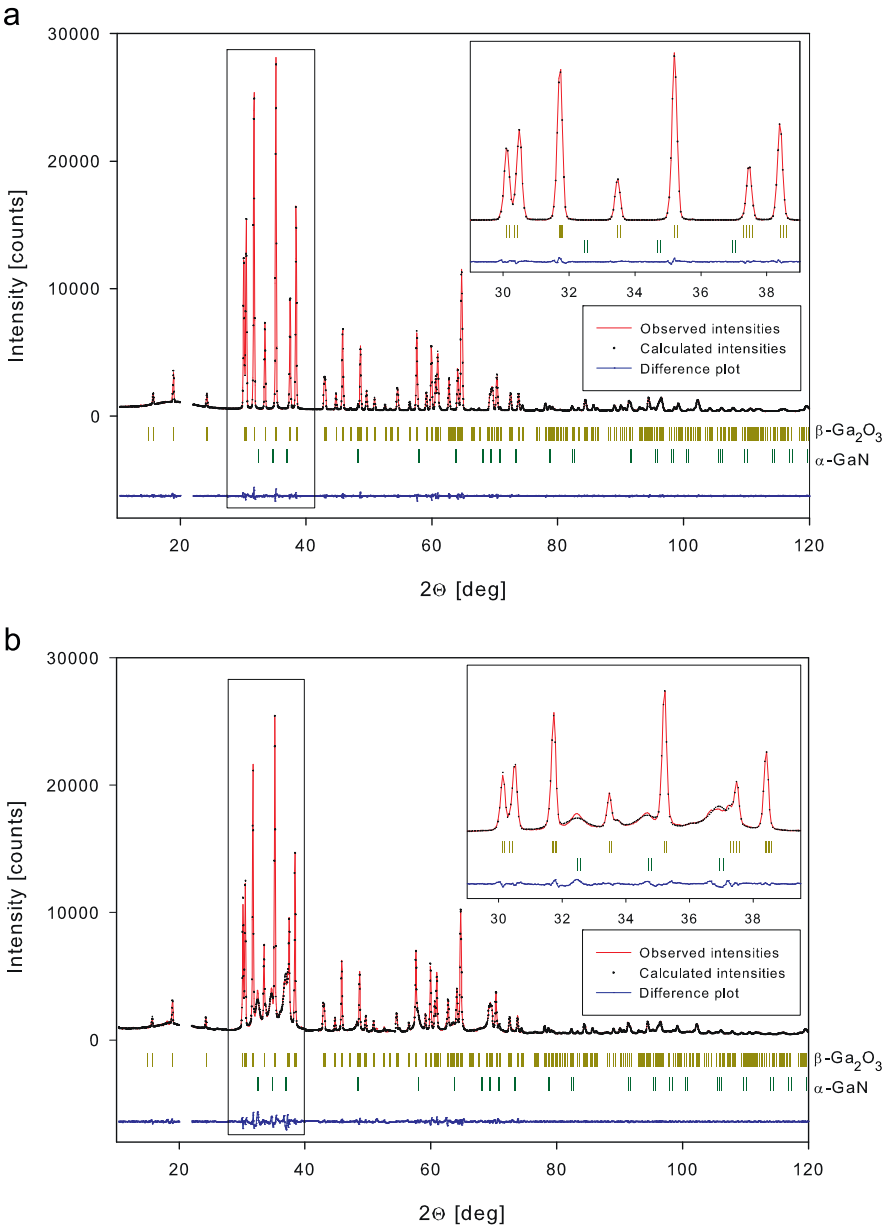

Fig. 4. Observed and refined XRD intensities of samples no. 2 (a) and no. 5 (b) which have been ammonolyzed at 600 °C for 3 and 24 h, respectively.

to the neutron diffraction data (see Section 3.2) and is consistent with our findings from TEM investigations [23]. The solubility of oxygen in wurtzite gallium nitride has already been researched extensively [7–14] and therefore no further detailed analysis of the nitride phase was performed.

Table 3 shows the summary of the refinements, and two typical refined patterns are shown in Fig. 4. The volume of the elementary cell and the lattice constants correspond to the β-Ga_2O_3 phase. There is no significant trend towards either expansion or contraction of any of the cell parameters or the volume of the elementary cell as a whole, even for the patterns which show a significant contribution of the emerging nitride phase. It has to be noted that due to the reasons cited above the refinement of sample no. 6 yields relatively inferior results when compared to the previous samples. Since the oxide content in this sample is close to the detection limit the values given for the cell parameters are more susceptible to systematic errors and far less stable than desired. Nevertheless, it is apparent, that the emergence of the broadened GaN reflections does not affect the quality of the refinement of the oxide phase.

Additionally to the experiments presented we conducted ammonolyses of β-Ga_2O_3 at temperatures of 530 and 650 °C for various reaction times up to 48 h and full conversion of the oxide phase. As before, the X-ray patterns of those series never revealed

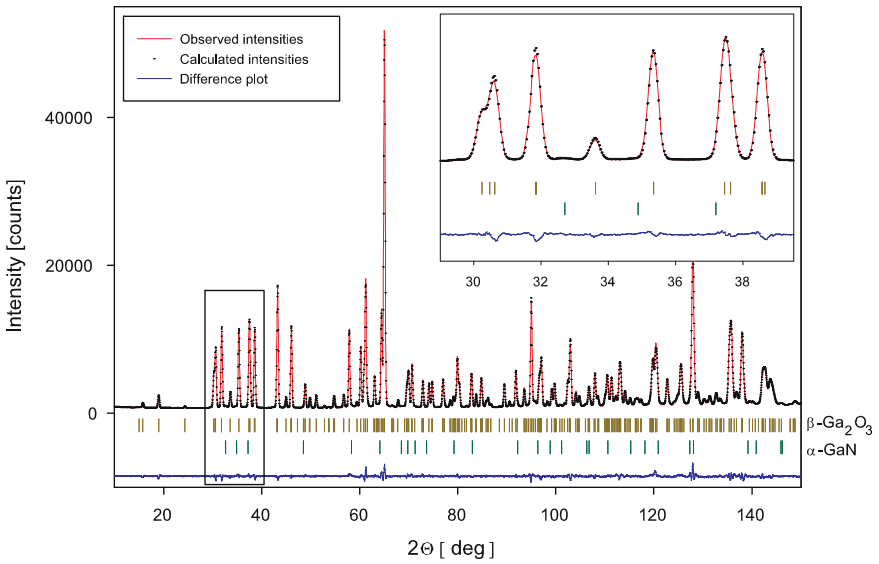

Fig. 5. Refinement of the neutron diffraction pattern of a sample that has been ammonolyzed at 780 °C for 30 min (sample 4 in Table 4). The inset shows a zoom into the 2θ region between 28° and 42°.

Table 4

(a) Effective anionic occupancy factors for the monoclinic β-Ga_2O_3 phase obtained from refinement of neutron diffraction data of samples ammonolyzed at 780 °C.

Sample	Ammonolysis duration at 780 °C [min]	Occ. O1	Occ. O2	Occ. O3
1	0	1.008(8)	1.006(6)	1.014(10)
2	5	1.010(8)	1.008(6)	1.014(10)
3	15	1.012(8)	1.004(6)	1.014(8)
4	30	1.012(8)	1.004(8)	1.014(8)
5	120	1.010(10)	0.996(10)	1.008(10)

(b) Summary of the refined cell parameters for the monoclinic β-Ga_2O_3 phase of samples ammonolyzed at 780 °C from neutron diffraction data.

Sample	Ammonolysis duration at 780 °C [min]	Rwp	χ^2	Cell volume [Å^3]	a [Å]	b [Å]	c [Å]
1	0	6.68	4.70	215.43749(53)	12.21620(10)	3.03839(2)	5.80419(2)
2	5	6.72	2.92	215.43958(22)	12.21656(12)	3.03833(2)	5.80419(5)
3	15	5.89	3.53	215.44498(90)	12.21629(09)	3.03840(2)	5.80433(5)
4	30	6.33	4.53	215.43644(53)	12.21620(10)	3.03837(3)	5.80420(5)
5	120	7.86	13.04	215.43124(70)	12.21561(15)	3.03848(3)	5.80413(6)

(c) Comparison of the molar fractions of the wurtzite GaN phase obtained from refinement of the neutron diffraction data and hot gas extraction (n.d.: not detectable) for samples that were ammonolyzed at 780 °C (n.d.: not detectable).

Sample	Ammonolysis duration at 780 °C [min]	Mol% GaN (obtained from refinement)	Wt% N (obtained from refinement)	Wt% N (obtained from hot gas extraction)
1	0	n.d.	n.d.	n.d.
2	5	n.d.	n.d.	n.d.
3	15	n.d.	n.d.	0.070(7)
4	30	8.59(0.68)	0.67(5)	0.50(5)
5	120	22.72(2.30)	1.94(19)	1.50(3)

any indication of phases other than β-Ga_2O_3 or α-GaN. We also note that the incubation time at the beginning of the reaction, with no detectable conversion (see Table 3), was already observed during our kinetic investigations by means of XAS [23] as is discussed there.

3.2. Neutron diffraction data and refinement

In contrast to the X-ray scattering factors of oxygen and nitrogen which are nearly identical, the coherent neutron scattering lengths are 9.370 fm for ^{14}N and 5.803 fm for ^{16}O, respectively [38], which yields a ratio of $f(^{14}N)/f(^{16}O)=1.615$. Thus, using neutrons it should be possible to detect any significant amount of nitrogen in the β-Ga_2O_3 lattice on any oxygen site or on interstitial sites, either randomly distributed or preferentially located on a specific site.

However, if the charge compensation for the nitrogen defects leads to the formation of oxygen vacancies (one oxygen vacancy for every two nitrogen defects, see Eq. (1)), the resulting effective anionic scattering factors would remain essentially unchanged (assuming a statistical distribution of N over all sites). In this case no direct information can be gained from the observation of the site occupancies alone. Though, the quantitative compensation of N by oxygen vacancies would lead to systematic changes of the lattice parameters and/or atomic positions with a trend as a function of the ammonolysis time. From our experimental data this case can be excluded within reasonable detection limits of a few mol% oxygen vacancies (see Tables 4a and b, Fig. 5).

In order to determine a value for the detection limit for nitrogen on any given oxygen site we simulated a series of neutron diffraction patterns of β-Ga_2O_3 with mixed anionic lattice occupation and increasing nitrogen content for each of the three oxygen positions (see Table 1). Those patterns were refined with the occupancy factors of each of the oxygen positions as the only free parameters. Since the scattering length for nitrogen is larger than the respective value for oxygen, the effective scattering factor on each position increases with increasing anion substitution. For 2% nitrogen on the anion sites we get a value for the effective occupancy factor whose increase is larger than the standard deviation obtained from the refinement of the experimental data (see Table 4a). Considering for the noise in the diffraction patterns, a value of 2–3% nitrogen substituted for oxygen, statistically distributed over all three oxygen positions or preferentially located on one specific anion site, seems to be a reasonable value for the detection limit above which any effect could be regarded as significant.

The refinements of the experimental diffraction patterns (see Fig. 5 as an example) show, however, no evidence of nitrogen on any site, even for the patterns that already exhibit contributions from the nitride. If the nitrogen atoms were positioned on previously empty, interstitial sites the powder pattern would show significant changes in the relative intensities even if symmetry was retained. This case can be ruled out by our data, which show the characteristic profile and intensity ratio of β-Ga_2O_3, with GaN being the only additional phase. In summary, the refined anionic occupancy factors of the oxide phase reveal no significant deviation from the theoretical value of 1 which represents a fully occupied position (see Table 4a). Since this is the case for all our samples we can rule out that a significant amount of nitrogen can be doped into the oxide phase by means of ammonolysis reaction at this temperature. This conclusion is supported by the fact that the obtained lattice parameters of the oxide phase (see Table 4b and Fig. 6) do not show any significant trend towards lattice expansion or contraction in agreement with the XRD data.

The nitrogen content of the ammonolyzed samples was also determined by hot gas extraction (see [39] for a description of the method). Very small amounts of nitrogen, close to the detection limit, were found for the samples which yield pure oxide diffraction patterns. For the GaN containing samples, the detected nitrogen content corresponds roughly to the N-amount due to the nitride as obtained from the refinement (see Table 4c).

Remembering that we had estimated the detection limit of nitrogen as 2–3 at%, we can now summarize the results of our X-ray and neutron diffraction experiments as follows: the solubility of nitrogen in β-Ga_2O_3 is definitely below 2–3 at%, in

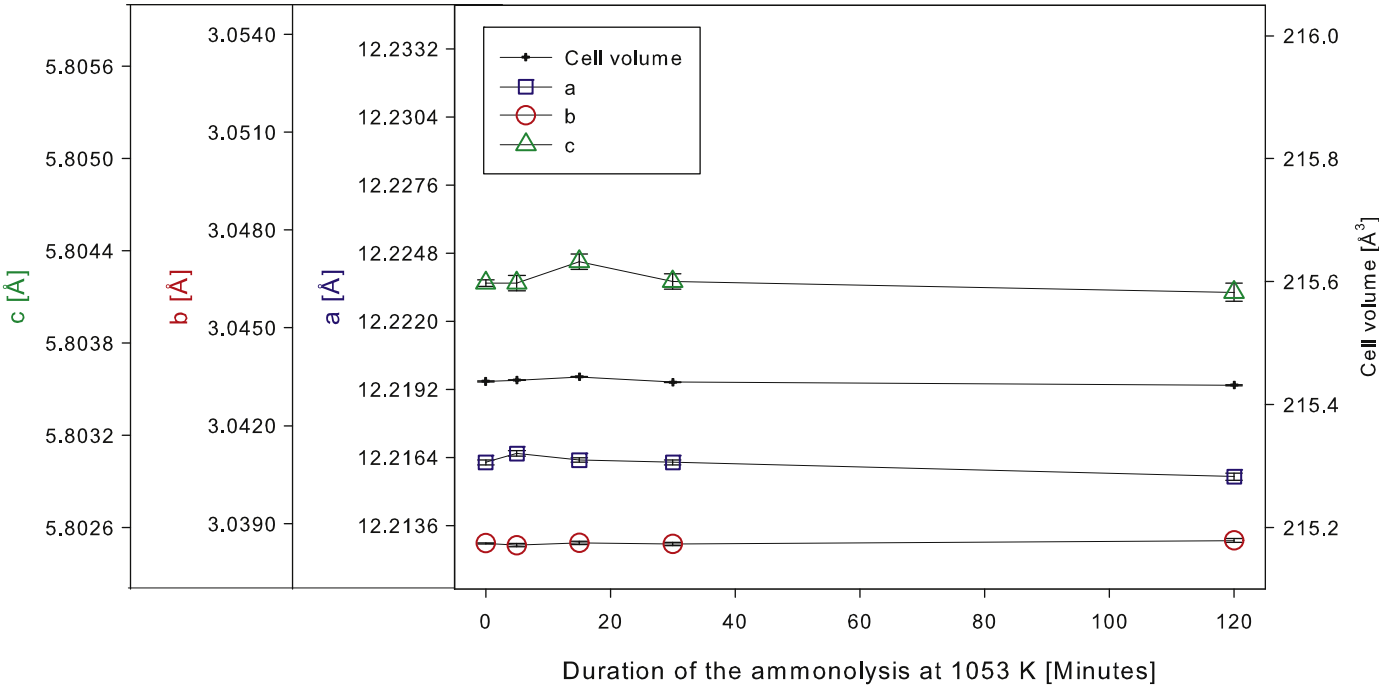

Fig. 6. Dependency of the refined cell parameters and cell volume of the β-Ga_2O_3 phase on the duration of the ammonolysis at 780 °C, as obtained from neutron diffraction data refinement.

strong contrast to the solubility of oxygen in the anion sublattice of GaN which can reach values of about 30 at% [13].

3.3. *In situ* X-ray absorption

The time development of the *in situ* XAS spectra during the ammonolysis shows a direct and continuous conversion from the initial β-Ga_2O_3 phase to the GaN product phase for all investigated temperatures [23]. As an example, in Fig. 7a the near edge region of the spectra is displayed, as in this region the development with time can be seen well. In Fig. 7b the radial distribution function that is obtained from the EXAFS part of the spectrum is shown. The resulting kinetics of the ammonolysis reaction was analyzed in detail in Ref. [23]. Here we focus on the aspect of identifying or excluding additional intermediate phases that may be crystalline or amorphous and on the structural aspects.

The time development of the radial distribution function around Ga in Fig. 7b reveals that the first coordination shell around Ga shifts to higher distances during the ammonolysis while the amplitude is slightly reduced. This is due to the change in the local Ga coordination during the conversion from β-Ga_2O_3 to GaN. In β-Ga_2O_3, Ga cations are surrounded by an average of 5 anions (mixed tetrahedral and octahedral coordination); while in wurtzite GaN each cation is tetrahedrally coordinated. The amplitude of the second coordination shell increases during the ammonolysis, which is a result of the nature of the second coordination shell in GaN and β-Ga_2O_3. In the nitride, there is a well defined 2nd coordination shell with 12 gallium neighbors at a distance of 3.18 Å, whereas in the oxide the 2nd shell is less well defined, with 20 gallium neighbors at a distance ranging from 3.04 to 3.44 Å.

To identify or exclude the presence of possible gallium oxynitrides as reaction intermediates, both the absorption coefficient $\mu(E)$ and the EXAFS function $\chi(k)$ are fitted with a linear combination of the α-GaN and β-Ga_2O_3 reference spectra according to Eqs. (3) and (4).

$$\mu(E) = a_\mu \cdot \mu(E)_{Ga_2O_3} + b_\mu \cdot \mu(E)_{GaN} \quad (3)$$

$$\chi(k) = a_\chi \cdot \chi(k)_{Ga_2O_3} + b_\chi \cdot \chi(k)_{GaN} \quad (4)$$

E and k are the energy and the wave vector, respectively, and a_μ, b_μ, a_χ and b_χ are the weighting factors. The fitting range in E-space ranges from 20 eV before to 50 eV after the edge. This conforms to a fit of the XANES region, which is sensitive to changes in the electronic structure of the samples during ammonolysis. The fits in k-space are done in a range from 2.5 to 9.0 $Å^{-1}$. This conforms to an EXAFS fit, which is sensitive to structural changes during the reaction. In Fig. 8a an experimental, normalized *in situ* spectrum (solid curve) and a fitted spectrum (dots) are plotted. The GaN- and the Ga_2O_3-contributions of the respective reference spectra to the whole fit and the residual are plotted below. One can see a

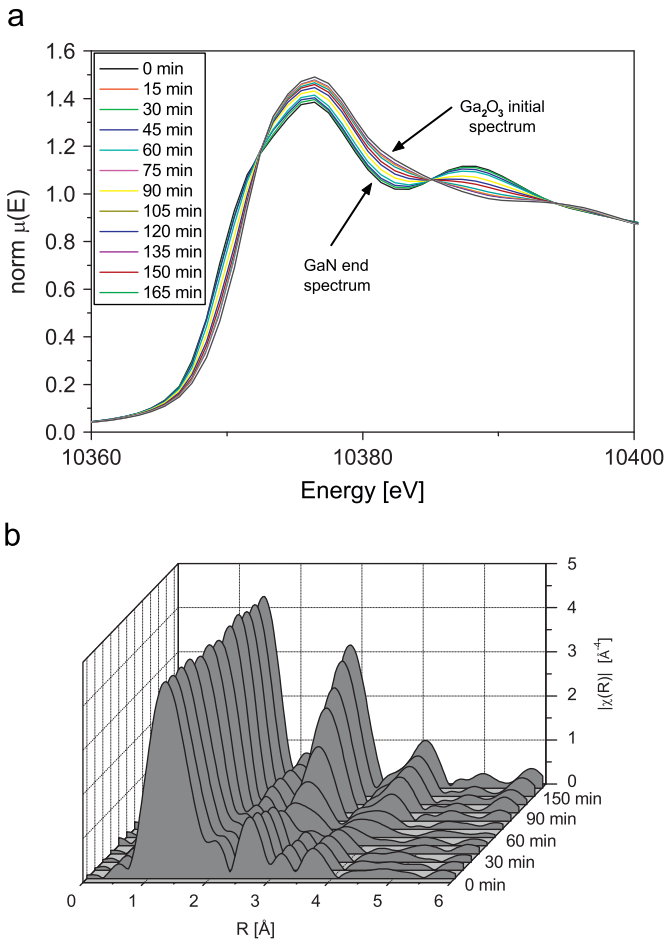

Fig. 7. Ammonolysis of β-Ga_2O_3 at 780 °C. Time development of the *in situ* XAS spectra in the near edge region of the Ga *K*-edge (a) and of the radial EXAFS distribution function (b) [23].

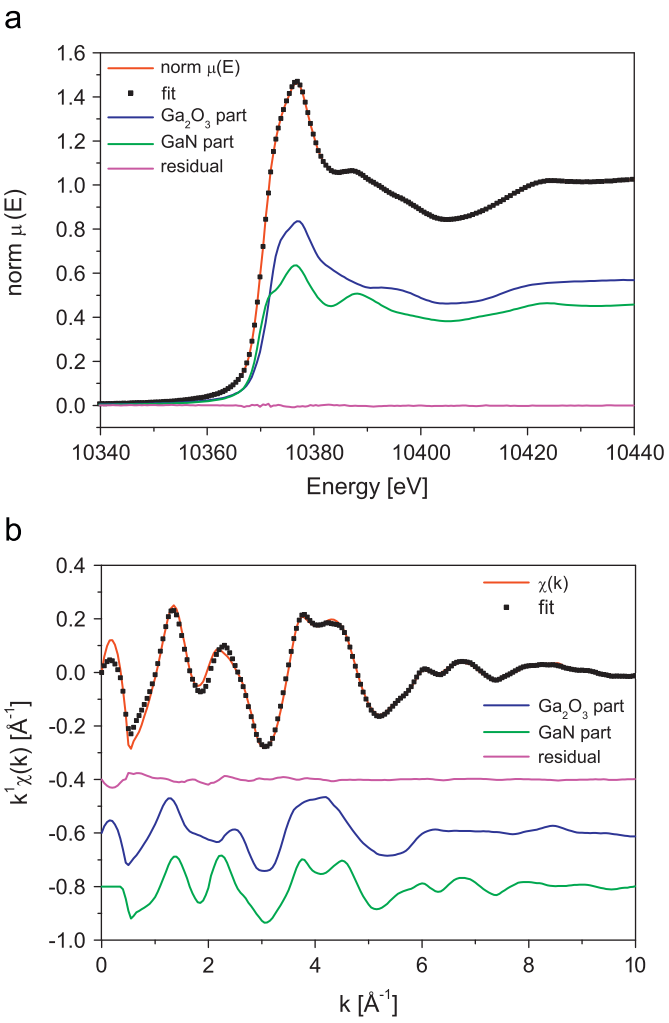

Fig. 8. Results of linear combination fits of X-ray absorption spectra taken during the ammonolysis at T=780 °C and t=80 min. (a) E-space (XANES region) according to Eq. (3), (b) k-space (EXAFS region) according to Eq. (4).

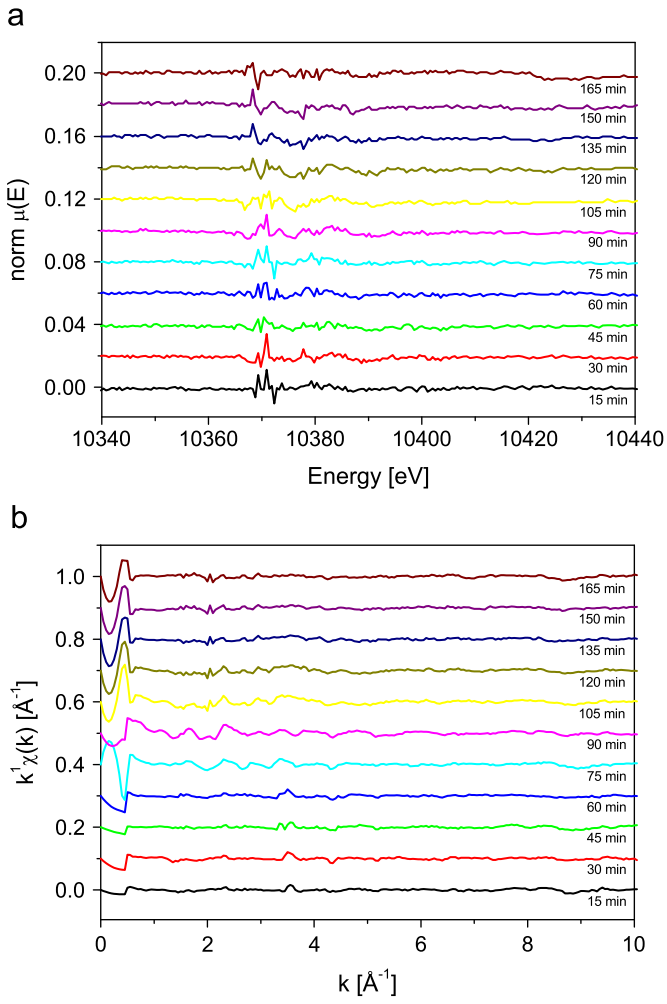

Fig. 9. Residuals of the fits in the XANES region in *E*-space (a) and the EXAFS region in *k*-space (b) of X-ray absorption spectra taken during the ammonolysis at $T = 780\,^{\circ}C$.

nearly perfect fit of the experimental curve. Thus, the XANES-region of the spectrum, corresponding to the electronic structure, can be described very well by a linear combination of the GaN and β-Ga_2O_3 reference spectra. Fig. 8b shows the fit in *k*-space. Again, the experimental curve is in very good agreement with the fit. Hence, the EXAFS-region of the spectrum, corresponding to the atomic structure of the sample, can be described by the same linear combination of α-GaN and β-Ga_2O_3 reference spectra as the XANES region.

In Fig. 9 the residuals for all fits of an *in situ* measurement are shown as function of time. They are small over the entire range and show no structural information. Therefore, we can rule out the presence of significant quantities of any crystalline or amorphous reaction intermediate during the ammonolysis of β-Ga_2O_3.

4. Conclusions

We examined the ammonolysis of β-Ga_2O_3 with gaseous NH_3 in the temperature range of 600–780 °C with *ex situ* X-ray and neutron diffraction and *in situ* X-ray absorption spectroscopy in order to investigate the oxygen-rich part of the system Ga_2O_3–GaN, with a particular focus on the existence of oxygen-rich oxynitrides and the solubility of nitrogen in β-Ga_2O_3.

XRD and neutron diffraction on samples quenched after ammonolysis show that β-Ga_2O_3 and α-GaN are the only crystalline phases that can be detected. All diffraction patterns are fully explained by the two binary compounds. From the refinement of XRD and neutron diffraction data we see no evidence of a significant change in the cell parameters of the oxide phase during the conversion which would be indicative for doping with nitrogen. In addition, we determined from the neutron diffraction data the effective occupancy factors of the oxygen positions in β-Ga_2O_3. Within the detection limit of this method (2–3%) we find no nitrogen dissolved within crystalline β-Ga_2O_3.

From the results of our *in situ* XAS experiments we can conclude that there are no detectable traces of either crystalline or amorphous intermediates during the ammonolysis of β-Ga_2O_3. Each of the spectra taken during the ammonolysis is fully explained by a mixture of the β-Ga_2O_3 and α-GaN spectra. It must be mentioned that this result was obtained in the XANES region as well as in the EXAFS region of the spectra, showing that the electronic structure as well as the atomic structure of the samples during the ammonolysis can be described well by a binary mixture of β-Ga_2O_3 and α-GaN only.

Acknowledgments

Financial support by the German Research Foundation (DFG Priority Program 1136) is gratefully acknowledged. The authors would like to express their gratitude to Dr. Anatoly Shenyshin and Dr. Markus Hoelzel (FRM-II, Garching) for their kind support during the neutron measurements at the SPODI diffractometer, Prof. Dr. M. Lerch (FU Berlin) for the quantitative analysis of nitrogen and oxygen via the hot gas extraction method, Prof. Dr. Gernot Heger, Prof. Dr. Georg Roth and Dr. Karine Sparta (AIXTAL, Aachen) for support in all crystallographic matters and Dr. E. Welter, Dr. K. Rickers, Dr. A. Webb and Dr. D. Zajac (all HASYLAB @ DESY) for support during the beam times.

References

[1] I. Akasaki, H. Amano, Jpn. J. Appl. Phys. 36 (1997) 5393.
[2] S. Nakamura, S. Pearton, G. Fasol, The Blue Laser Diode. The Complete Story, Springer, Berlin, 2000.
[3] M. Fleischer, H. Meixner, J. Appl. Phys. 74 (1993) 300.
[4] M.R. Lorenz, J.F. Woods, R.J. Gambino, J. Phys. Chem. Solids 28 (1976) 403.
[5] T. Harwig, G.J. Wubs, G.J. Dirksen, Solid State Commun. 18 (1976) 1223.
[6] I. Kinski, F. Scheiba, R. Riedel, Adv. Eng. Mater. 7 (2005) 921.
[7] G.A. Slack, L.J. Schowalter, D. Morelli, J.A. Freitas Jr., J. Cryst. Growth 246 (2002) 287.
[8] W.M. Chen, I.A. Buyanova, M. Wagner, B. Monemar, J.L. Lindstrom, H. Amano, I. Akasaki, MRS Internet J. Nitride Semicond. Res. (4S1, G5.4) (1999).
[9] C. Wetzel, H. Amano, I. Akasaki, J.W. Ager, I. Grzegory, B.K. Meyer, Physica B 302–303 (2001) 23.
[10] R.Y. Korotkov, B.W. Wessels, MRS Internet J. Nitride Semicond. Res. (5S1, W3.80) (2000).
[11] B.C. Chung, M. Gershenzon, J. Appl. Phys. 72 (1992) 651.
[12] C.G. Van de Walle, Phys. Rev. B 68 (2003) 165209.
[13] J.I. Pankove, in: K.J. Bachmann, H.L. Wang, C. Schwab (Eds.), Non-Stoichiometry in Semiconductors, Elsevier Science, 1992.
[14] S. Hautakangas, V. Ranki, I.M.J. Puska, K. Saarinen, L. Liszkay, D. Seghier, H.P. Gislason, J.A. Freitas Jr., R.L. Henry, X. Xu, D.C. Look, Physica B 376–377 (2006) 424.
[15] M. Puchinger, D.J. Kisailus, F.F. Lange, T. Wagner, J. Cryst. Growth 245 (2002) 219.
[16] P. Kroll, Phys. Rev. B 72 (2005) 144407.
[17] P. Kroll, R. Dronskowski, M. Martin, J. Mater. Chem. 15 (2005) 3296.
[18] E. Soignard, D. Machon, P.F. McMillan, J. Dong, B. Xu, K. Leinenweber, Chem. Mater. 17 (2005) 5465.
[19] I. Kinski, G. Miehe, G. Heymann, R. Theissmann, R. Riedel, H. Huppertz, Z. Naturforsch. 60b (2005) 831.
[20] W.S. Jung, Bull. Korean Chem. Soc. 25 (2004) 51.
[21] W.S. Jung, Mater. Lett. 60 (2006) 2954.
[22] L. Nagarajan, R.A. De Souza, D. Samuelis, I. Valov, A. Börger, J. Janek, K.D. Becker, P.C. Schmidt, M. Martin, Nat. Mater. 7 (2008) 391.

[23] J. Brendt, D. Samuelis, T.E. Weirich, M. Martin, Phys. Chem. Chem. Phys. 11 (2009) 3127.
[24] M.R. Lorenz, J.F. Woods, R.J. Gambino, J. Phys. Chem. Solids 28 (1967) 403.
[25] R. Roy, V.G. Hill, E.F. Osborn, J. Am. Chem. Soc. 74 (1952) 719.
[26] M. Zinkevich, F. Aldinger, J. Am. Ceram. Soc. 87 (2004) 683.
[27] J. Åhman, G. Svensson, J. Albertsson, Acta Cryst. C 52 (1996) 1336.
[28] A.V. Davydov, T.J. Anderson, in: T.D. Moustakas, S.E. Mohney, S.J. Pearton (Eds.), III–V Nitride Materials and Processes III, ECS, Boston, MA, 1998, p. 38 (PV 98-18).
[29] R. Juza, H. Hahn, Z. Anorg. Allg. Chem. 239 (1938) 282.
[30] Y.J. Park, C.S. Oh, T.H. Yeom, Y.M. Yu, J. Cryst. Growth 264 (2004) 1.
[31] J. Rodriguez-Carvajal, Physica B 192 (1993) 55.
[32] U. Koops, D. Hesse, M. Martin, J. Mater. Res. 17 (2002) 2489.
[33] N. Hilbrandt, M. Martin, J. Synchr. Rad. 6 (1999) 489.
[34] R. Frahm, Rev. Sci. Instrum. 60 (1989) 2515.
[35] B. Ravel, Athena User's Guide 1.0, 2007.
[36] D.C. Koningsberger, R. Prins, X-Ray Absorption: Principles, Applications, Techniques of EXAFS, SEXAFS and XANES, Wiley-Interscience, New York, 1988.
[37] M. Newville, P. Livins, Y. Yacoby, J.J. Rehr, E.A. Stern, Phys. Rev. B 47 (1993) 14126.
[38] V.F. Sears, Neutron News 3 (3) (1992) 29.
[39] S. Nakhal, Thesis, University of Berlin, 2008.